Conformal anomaly in finite-temperature magnetic response of one-dimensional spin systems

C. Northe [1,2,*] C. Zhang,[1,2,*] R. Wawrzyńczak [3] J. Gooth,[2,3] S. Galeski,[3] and E. M. Hankiewicz[1,2]

[1]*Institute for Theoretical Physics and Astrophysics, Julius-Maximilians-Universität Würzburg, 97074 Würzburg, Germany*
[2]*Würzburg-Dresden Cluster of Excellence ct.qmat, Physikalisches Institut,*
Julius-Maximilians-Universität Würzburg, 97074 Würzburg, Germany
[3]*Max Planck Institute for Chemical Physics of Solids, Nöthnitzer Straße 40, 01187 Dresden, Germany*

The conformal anomaly indicates the breaking of conformal symmetry (angle-preserving transformations) in quantum theory by quantum fluctuations, and is a close cousin of the gravitational anomaly. We show that the conformal anomaly controls the variance of the local magnetization M_{loc} at finite temperatures in spin chains and spin ladders. This effect is predicted to appear at constant and variable temperature across the sample. The change of M_{loc} induced by the conformal anomaly is of the order of 3–5% of angular momentum $\hbar/2$ at 1 K for $(C_7H_{10}N)_2CuBr_4$ (DIMPY) or copper pyrazine nitrate (CuPzN) and increases linearly with temperature. Further, for a temperature gradient of 10% across the sample, the time relaxation of the nonequilibrium M_{loc} is of the order of nanoseconds. Thus, we believe that experimental techniques such as neutron scattering, nuclear magnetic resonance (NMR), spin noise, and ultrafast laser pumping should determine the presence of the conformal anomaly. Therefore, we outline a method to detect the conformal anomaly in spin observables of strongly interacting low-dimensional magnets.

I. INTRODUCTION

The study of quantum anomalies is one of the most rapidly developing fields at the interface between condensed matter experiment and high-energy theory. A quantum anomaly is a violation of classical conservation laws due to quantum fluctuations. Understanding such conservation law violations has played an important role in the development of the standard model. However, experimental access to these phenomena is often hindered by the extremely high energies required in particle physics experiments. Recently, such anomalies have been accessed and experimentally studied in Weyl and Dirac semimetals. This new direction in the study of solids resulted in recent observations of signatures of the chiral [1–6] and mixed axial-gravitational [7] anomaly manifesting as additional field-dependent contributions to the longitudinal components of the conductance and thermoelectric conductance tensors.

Thus far experimental studies of quantum anomalies in solids have mainly focused on signatures of anomalies in nearly free electron systems such as the Weyl semimetals. However, anomalies also play a role in strongly correlated systems, where interactions cannot be treated as a simple perturbation to the physics of free quasiparticles. In this article, we study strongly interacting spin chain systems using quantum field theory to predict experimental signatures of the conformal anomaly. Conformal symmetry plays an important role in many branches of physics including string theory [8], quantum entanglement [9,10], holography [11], topologically ordered phases [12,13], and symmetry-protected topological phases [14], and it guides our understanding of universality and criticality [15–17].

Knowledge of the conformal anomaly of a system near criticality helps in determining the conformal field theory (CFT) describing the critical point. More precisely, the anomaly itself is the phenomenon of symmetry breaking upon quantization and it is quantified by the so-called left- and right-moving central charges, c and $\bar{c}$, respectively. These numbers quantify the amount of left- and right-moving degrees of freedom, respectively. They are characteristic of any $(1+1)$-dimensional CFT. For instance, a Tomonaga-Luttinger liquid (TLL) has $c = \bar{c} = 1$ while the Ising model, at its crititcal point, has $c = \bar{c} = 1/2$. Therefore, one can say that the Ising CFT has half as many degrees of freedom as the TLL. As such, the conformal anomaly distinguishes between different classes of CFTs and vastly narrows down the set of candidate CFTs describing the critical point.

In this article, we predict consequences of the conformal anomaly for magnetic properties of strongly interacting one-dimensional (1D) Heisenberg spin-1/2 chains and ladders. Recent studies of 1D quantum magnets have shown that the ground states of both the Heisenberg spin-1/2 chain and the magnetized spin-1/2 ladder belong to the universality class of the TLL [18–20]. The TLL, due to its one-dimensionality and divergence of susceptibilities, lives at the verge of an ordering instability, making it a realization of the $z = 1$ quantum critical state. As such the TLL is expected to exhibit no internal energy scales apart from temperature, and thus features the conformal anomaly. Indeed the free energy of quantum critical systems [21,22] was discussed in the context of the conformal anomaly; however, those works focus on the appearance of the conformal anomaly in thermodynamic properties such as specific heat [22] and thermal conductivity [23]. In addition,
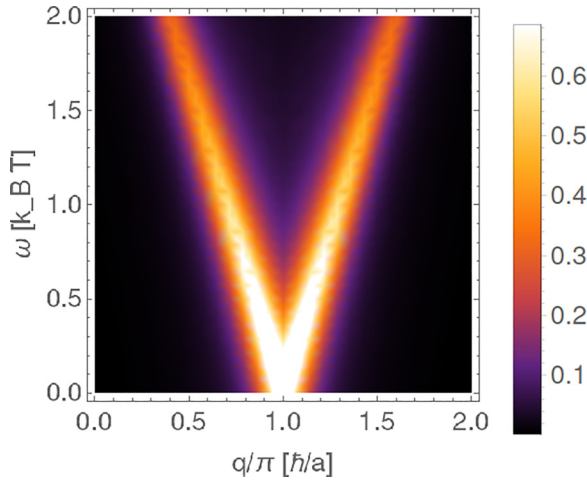
---

*These two authors contributed equally to this work.

FIG. 1. Plot of spin susceptibility $Q_T(k, \omega)$ at $T = 15$ K, in units of $a^2\hbar^2 K/\pi$. The Dirac delta distribution in Eq. (C5) is represented by $\frac{\eta/\pi}{(\omega^2+\eta^2)}$ with $\eta = 0.3k_BT$ in this plot. Note that, due to the antiferromagnetic interaction, this plot is shifted in a magnetic Brillouin zone $\pi\hbar/a$ in momentum.
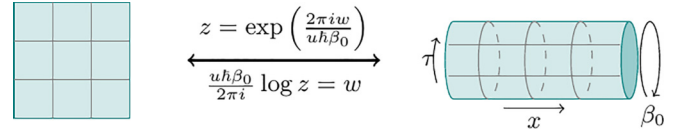

FIG. 2. Conformal transformations are angle-preserving transformations, as indicated by the grids. The transformation here relates a zero-temperature system, drawn as plane, to a thermal ensemble at temperature T, depicted by a cylinder of circumference $\beta_0 = (k_B/T)^{-1}$.

thermal effects for curved space were connected to the conformal anomaly in [24–26], which are difficult to observe in experiments. Altogether, to date there exist no predictions on how the conformal anomaly is manifested in spin observables. However, rapid development of spectroscopic techniques and growth of excellent material realizations of low-dimensional magnetic Hamiltonians [27–33] has opened a new avenue for observation of signatures of the conformal anomaly in flat spacetime by directly investigating spin observables.

In this article, we analyze (quasi)one-dimensional spin chains and extract the central charge, which characterizes the conformal anomaly, from the magnetic properties of these materials. Gapless dispersion relations, as read out from the spin susceptiblity in Fig. 1, are a requirement for conformal symmetry. Moreover, the Fourier transform of the spin susceptibility gives the value of the central charge. Furthermore, we predict new signatures of the conformal anomaly at finite temperatures, such as an energy-integrated structure factor combined with the local on-site variance of magnetization. We perform analyses for equilibrium states at finite temperature, but also for nonequilibrium states with varying temperature profiles. In particular, we show that the local variance of magnetization scales linearly with the temperature and can be measurable in many quasi-1D materials such as $(C_7H_{10}N)_2CuBr_4$ (DIMPY) and copper pyrazine nitrate (CuPzN). We identify how these new quantities can be measured in neutron scattering, NMR, atomic force microscopy (AFM) and spin noise. Moreover, we predict that the dynamics of the local magnetization should lie in the range of nanoseconds, and thus it is accessible in ultrafast laser spectroscopy.

II. PREREQUISITES

A. A brief introduction to the conformal anomaly

The conformal anomaly is associated with conformal symmetry, which is a hallmark of a system at criticality.

Such systems are classically invariant under angle-preserving transformations as seen in Fig. 2 for a transformation relating the infinite plane, parameterized by complex coordinates $(z, \bar{z})$, to a cylinder, parameterized by complex coordinates $(w, \bar{w})$. The plane can be thought of as a zero-temperature setup, while the cylinder carries the interpretation of a system at temperature $T = (k_B\beta_0)^{-1}$. Physically, the cylinder coordinates $(w = u\tau - ix, \bar{w} = u\tau + ix)$ decompose into the spatial coordinate of the physical system $x \in \mathbb{R}$ and a compact Euclidean temporal coordinate $\tau \in [0, \hbar\beta_0]$, with u being the velocity of the bosonic quasiparticles. Temperature introduces a scale, to which the quantized critical system responds via the conformal anomaly, or more precisely the central charge. This is seen in the expectation value of the left-moving and right-moving components of the energy-momentum tensor, which vanish at zero temperature, $\langle T \rangle = 0 = \langle \bar{T} \rangle$. Upon thermally exciting the system via the conformal transformation $z = \exp(\frac{2\pi i w}{u\hbar\beta_0})$, a shift in energy controlled by the central charges c and $\bar{c}$ occurs,

$$\langle T(w) \rangle_{\beta_0} = \frac{\pi^2 c}{6u\hbar\beta_0^2}, \quad \langle \bar{T}(\bar{w}) \rangle_{\beta_0} = \frac{\pi^2 \bar{c}}{6u\hbar\beta_0^2}, \quad (1)$$

as reviewed in Appendix A. In general $\bar{c} \neq c$; however, in the systems of interest in this manuscript we have $c = \bar{c}$. This brief introduction reveals a physical aspect of the conformal anomaly. Whenever a macroscopic scale is introduced to the CFT, as exemplified in Eq. (1) with temperature [34], the CFT responds with the central charge, i.e., by the conformal anomaly.

B. Spin models

The models of interest to us are 1D spin systems of length L, such as a spin-$\frac{1}{2}$ chain with Hamiltonian $H_{SC} = \sum_i[J \sum_{b=x,y} S_i^b S_{i+1}^b + J_z S_i^z S_{i+1}^z - BS_i^z]$ where B is a magnetic field perpendicular to the chain. The system size L is chosen much larger than the lattice constant a. If $J_z = J_\perp$, the Hamiltonian H_{SC} becomes that of the Heisenberg chain, $H_{HC} = J \sum_i(\vec{S}_i \cdot \vec{S}_i - BS_i^z)$. The spin-$z$ operator bosonizes according to [19,20]

$$\frac{S^z(x)}{a\hbar} = m\mathbf{1} - \frac{\partial_x\varphi}{2\pi R} + \frac{1}{\pi}\cos\left(\frac{\varphi(x)}{R} - 2k_F(h)x\right), \quad (2)$$

where the compactification radius $R = \frac{1}{\sqrt{4\pi K}}$ is related to the Luttinger parameter $K = \frac{\pi}{2(\pi-\chi)}$, $u = \frac{\pi}{2}\frac{\sin\chi}{\chi}$ [35] is the velocity of the bosonic quasiparticles with $\cos\chi = J_z/J$, and $k_F(h) = k_F + \pi m$ is the Fermi momentum shifted by the magnetization per site, $m = \langle S^z(x)\rangle/L$. Note that the bosonic

velocity u does not equal the Fermi velocity v_F. In this paper we are not concerned with the ladder operators $S^{\pm}$, and thus we omit their bosonization prescription. The spin chain Hamiltonian H_{SC} reduces to that of the TLL [19,20], $H_{TLL} = \frac{\hbar u}{2} \int dx [(\partial_x \varphi)^2 / K + K(\partial_x \theta)^2]$ up to terms irrelevant in the renormalization group sense. This system is classically conformally invariant. However, upon quantization it features the conformal anomaly, which we exploit below.

A more elaborate case of a 1D spin system is a spin ladder, in which two spin-$\frac{1}{2}$ Heisenberg chains, i.e., with $J_z = J$ in their Hamiltonian H_{HC}, are coupled to each other via an interaction term $H_{ladder} = H_{HC}^{(1)} + H_{HC}^{(2)} + J_\perp \sum_i \vec{S}_i^{(1)} \cdot \vec{S}_i^{(2)}$. The superscripts indicate the respective chain and we have chosen a magnetic field aligned with the total spin in the z direction. This model possesses magnon excitations which furnish a spin triplet. At zero magnetic field these excitations are degenerate and gapped. Upon turning on a magnetic field, the Zeeman splitting of the triplet moves one of the magnons closer to zero energy. At a critical magnetic field B_{crit}, this mode becomes gapless. In the low-energy limit, attention is restricted to this degree of freedom, which is described by the TLL Hamiltonian H_{TLL} [36], so long as $J_\perp \ll J$. The bosonization of the S^z operator takes the same shape as (2), but with different numerical values for the Luttinger parameter K (and u) [36].

III. CONFORMAL ANOMALY IN THERMAL SPIN CORRELATORS

A. Constant temperature

As explained in the Introduction, the anomaly resides with the energy-momentum tensor, which in the bosonic TLL language is given by a point splitting procedure,

$$\frac{T(w)}{2\pi u \hbar} = -\lim_{w' \to w} \left[\partial \varphi(w') \partial \varphi(w) + \frac{1}{4\pi (w - w')^2} \right], \quad (3)$$

where $\partial = \partial_w$. A similar expression holds for $\bar{T}(\bar{w})$. This makes clear, together with (1), that the thermal correlator

$$\langle \partial \varphi(w) \partial \varphi(w') \rangle_{\beta_0}$$

$$\stackrel{w' \to w}{=} -\frac{1}{4\pi (w - w')^2} - \frac{\pi}{12(u \hbar \beta_0)^2} + \mathcal{O}(w - w') \quad (4)$$

contains the central charge. Indeed, taking an expectation value at inverse temperature β_0 of (3) and plugging (4) into it, the thermal expectation value (1) is readily recovered, along with the well known values $c = 1 = \bar{c}$ for the TLL.

Since the S^z operator (2) contains $\partial \varphi$, the central charge must reside in the Green's function

$$G_{\beta_0}(\xi_1; \xi_2) = \langle S^z(\xi_1) S^z(\xi_2) \rangle_{\beta_0} - \langle S^z(\xi_1) \rangle_{\beta_0} \langle S^z(\xi_2) \rangle_{\beta_0}, \quad (5)$$

where we introduce the spacetime label $\xi = (\tau, x) = (w, \bar{w})$ for observables containing both w and $\bar{w}$ dependence. This correlator is evaluated explicitly in Appendix B.

If the system has translation symmetry, the Green's function $G_{\beta_0}(\xi_1; \xi_2)$ can be simplified to $G_{\beta_0}(\xi_1 - \xi_2)$. The Fourier transformation of Eq. (5) is denoted by spin susceptibility $Q_T(k, \omega)$:

$$Q_T(k, \omega) = \iint G_{\beta_0}(x, t) e^{-ikx + i\omega t} dx \, dt. \quad (6)$$

The spin susceptibility $Q_T(k, \omega)$, is plotted in Fig. 1 and explored in depth in the next section. As we show below, integrating the data of the plot over momentum q and frequency ω, one obtains the central charge.

In order to extract the central charge similar to (4), the coincidence limit $\xi_2 \to \xi_1$ needs to be taken in $G_{\beta_0}(\xi_1; \xi_2)$, which is, however, divergent and a regularization is required. We choose to subtract the zero temperature value, i.e., at $\beta_0 \to \infty$, taken as well in the coincidence limit, providing the normalized variance of local magnetization,

$$M_{loc}^2(\xi, \beta_0) = \lim_{\xi' \to \xi} [G_{\beta_0}(\xi'; \xi) - G_\infty(\xi'; \xi)]/S_{max}^2, \quad (7)$$

where $S_{max} = \frac{\hbar}{2}$ is the magnitude of the spin. It measures how much the variance of local magnetization in the z direction deviates at fixed temperature β_0 from its value at zero temperature. Note that M_{loc}^2 is dimensionless, and its square root M_{loc} is the standard deviation in statistics. A careful evaluation of the limit (7), which is shown in detail in Eq. (B7) of Appendix B, yields [37]

$$M_{loc}^2(\xi, \beta_0) = \frac{2Ka^2}{\pi^2 u \hbar} [\langle T(w) \rangle_{\beta_0} + \langle \bar{T}(\bar{w}) \rangle_{\beta_0}]$$

$$= \frac{Ka^2}{3(u \hbar \beta_0)^2} (c + \bar{c}), \quad (8)$$

where (1) has been plugged into the second equality. For the TLL one has $c = \bar{c} = 1$. In the second line of the above equations, the translation symmetry is assumed. In this case, the variance of local magnetization M_{loc}^2 only depends on the temperature and will be denoted by $M_{loc}^2(\beta_0)$ for simplicity. This is the first main result of this article. The attentive reader might have noticed that the cosine term in (2) does not contribute to (8), as demonstrated in (B7) of Appendix B. This is due to the limit $\xi' \to \xi$ in the local magnetization (7). It removes all but the nonconstant orders in the product $S^z(\xi_1) S^z(\xi_2)$, of which the cosine term contributes none in the situations studied here, as shown in Appendix B.

Modeling the spin ladder material DIMPY [(C$_7$H$_{10}$N)$_2$CuBr$_4$] by H_{ladder}, one has $a = 7.51$ Å, and the TLL parameters at $B \approx 8.7$ T (tesla) are $K \approx 1.2$, $u\hbar/a \approx 2.34$ meV [38]. This yields $M_{loc}^2 = 1.1 \times 10^{-3} (T/K)^2$, where K stands for kelvin (and T for temperature). At $B \approx 20$T, one has $K \approx 1.2$, $u\hbar/a \approx 1.62$ meV, giving $M_{loc}^2 = 2.3 \times 10^{-3} (T/K)^2$. For the Heisenberg spin chain material copper pyrazine dinitrate (CuPzN) [33,39], one has $a = 6.7$ Å, $J = 0.9$ meV and TLL parameters $K = 1/2$, $\hbar u = J a \pi / 2$. This yields $M_{loc}^2 = 1.2 \times 10^{-3} (T/K)^2$. These results are plotted in Fig. 3. The experimental detection of $M_{loc}^2(\xi, \beta_0)$ is discussed below; see Eqs. (18) and (19).

B. Temperature gradients and M_{loc}^2

The signal (8) can be amplified by preparing the system in a nonequilibrium initial state defined by a nonconstant temperature profile $\beta(x)$ interpolating between constant values $\beta_{L,R} = (k_B T_{L,R})^{-1}$ at the left and right extremes of the sample, with a kink at $x = 0$ [24,40,41]. One example of such
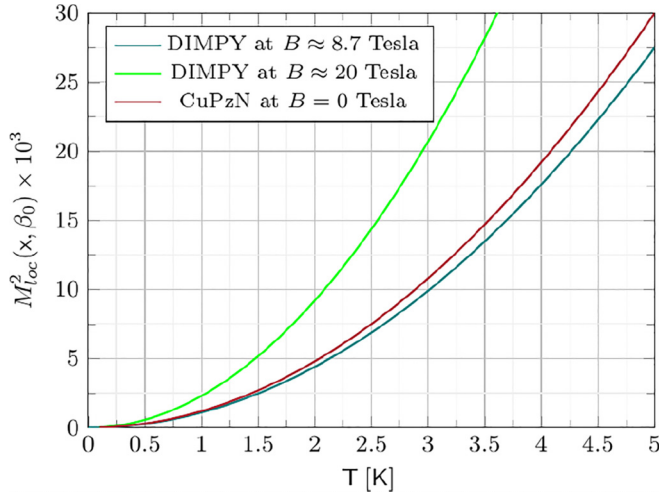
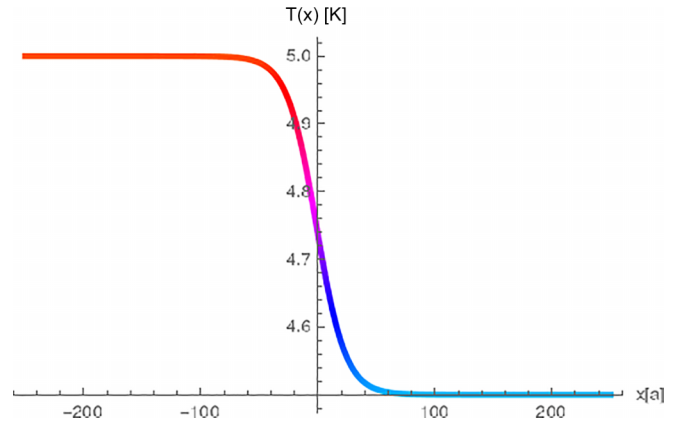FIG. 3. Normalized variance of local magnetization $M_{\text{loc}}^2(\xi, \beta_0)$ for DIMPY and CuPzN.

FIG. 4. A nonequilibrium temperature profile $T_1(x) = 1/[k_B \beta_1(x)]$ based on (9) is plotted for $T_L = 5$ K and $T_R = 4.5$ K. The sample size is chosen to be $\ell = 250a$ and the rate of temperature change is $\delta = 0.1\ell$.

a temperature profile is given in [40]

$$\beta_1(x) = \tfrac{1}{2}\{\beta_L + \beta_R - (\beta_L - \beta_R)\tanh[x/\delta]\}, \qquad (9)$$

where δ indicates the rate of temperature change across the sample. This profile is plotted in Fig. 4. It is convenient to introduce an effective sample size ℓ, beyond which the temperature profile is saturated at its asymptotic values $\beta_{L/R}$. Since the temperature profile is controlled by the new length scale δ, so is ℓ. In Fig. 4 one can choose $\ell = 250a$, where a is the lattice constant and $\delta = 0.1\ell$. Since this is the actual length scale relevant to our analysis, we refer to ℓ as the sample size.

In this section, we revert to real time, $\tau = it$ so that $w = i(ut - x)$ and rotate this onto the real line, $w_- = iw$ and $w_+ = -i\bar{w}$, resulting in light-cone coordinates $w_\pm = x \pm ut$. Moreover, all results we present in this section are valid only in the thermodynamic limit, which means that the actual sample size $L \to \infty$.

In the language of the previous sections a nonconstant temperature profile is depicted as deformed cylinder, viz., Fig. 5. A conformal mapping

$$y_\pm = f(w_\pm) = \int_0^{w_\pm} \beta_{\text{av}}/\beta(s)\,ds \qquad (10)$$

reshapes this cylinder into one with uniform radius β_{av}, corresponding to a system of constant average temperature $(k_B \beta_{\text{av}})^{-1} = (T_L + T_R)/2$. The new coordinates $y_\pm$ are naturally adapted to the symmetries of the system, similarly to how spherical problems are best handled in polar coordinates. Indeed, the transformation $y_\pm$ shows that the deformed cylinder has the same amount of symmetries as the case of uniform temperature, described in the previous section.

As derived in [40], the expectation value of the energy-momentum tensor becomes

$$\langle T_\pm(w_\pm)\rangle_{\beta(\xi)} = \frac{\pi^2 \mathsf{c}}{6u\hbar\beta(w_\pm)^2} - \frac{u\hbar\mathsf{c}}{12}Sf(w_\pm), \qquad (11)$$

with Schwarzian derivative $Sf(s) = \frac{1}{2}[\beta'(s)/\beta(s)]^2 - \beta''(s)/\beta(s)$. Evaluated on the profile (9), for instance, the Schwarzian becomes

$$Sf_1(x) = \frac{(\beta_L - \beta_R)}{\cosh^4\left(\frac{2x}{\delta}\right)}\frac{\beta_R - \beta_L + 2(\beta_L - \beta_R)\cosh\left(\frac{2x}{\delta}\right) - 2(\beta_L + \beta_R)\sinh\left(\frac{2x}{\delta}\right)}{2\delta^2\left[\beta_L + \beta_R + (\beta_R - \beta_L)\tanh\left(\frac{x}{\delta}\right)\right]^2}. \qquad (12)$$

By removing the rate of temperature change, i.e., $\delta \to \infty$, we see that the temperature profile (9) becomes trivial and the Schwarzian (12) disappears. Equation (11) then reduces to (1). For finite δ, (11) shows that a nontrivial temperature profile introduces a new macroscopic scale δ or equivalently ℓ in the CFT. Indeed, comparing with the case of constant temperature, where $\langle T\rangle_{\beta_0} \propto \mathsf{c}/\beta_0^2$, there is an additional Schwarzian contribution in (11), which is proportional to c/δ^2.

As explained in Appendix A, the derivation of M_{loc}^2 is entirely analogous to the case of constant temperature and thus $M_{\text{loc}}^2(\xi, \beta(\xi))$ is obtained by simply inserting (11)

into (8),

$$M_{\text{loc}}^2(\xi, \beta(\xi)) = \frac{2Ka^2}{\pi^2\hbar u}\sum_{\sigma=\pm}\left[\frac{\pi^2 \mathsf{c}}{6u\hbar\beta(w_\sigma)^2} - \frac{u\hbar\mathsf{c}}{12}Sf(w_\sigma)\right]. \qquad (13)$$

This is the second main result of this article. It shows that the lack of translation invariance in the spatial direction due to $\beta(x)$ also induces time dependence in M_{loc}^2, as visualized in Fig. 6 for CuPzN. At the hot (cold) extreme of the sample, depicted in red (blue), $M_{\text{loc}}^2(\xi, \beta(x)) = M_{\text{loc}}^2(\xi, \beta_{L(R)})$. At $t > 0$
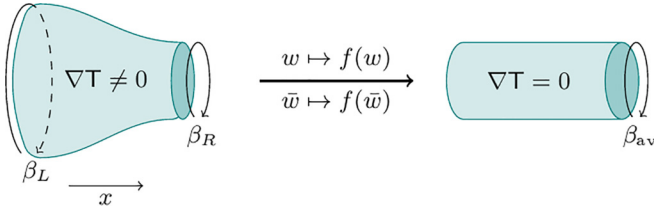
FIG. 5. In the Euclidean setting, a smooth, nonconstant temperature profile may be seen as a deformed cylinder with two distinct circumferences $\beta_{L,R}$ at its ends. This can be mapped into a system of constant average inverse temperature β_{av} by the conformal transformation $y_\pm = f(w_\pm) = \int_0^{w_\pm} \beta_{av}/\beta(s)ds$.

the peak separates in two waves which leave behind an equilibrated region (pink) for which $M_{loc}^2(\xi, \beta(\xi)) = M_{loc}^2(\xi, \beta_{av})$. M_{loc}^2 is strongest in the vicinity of $x = 0$ when $t = 0$, where the magnitude of $M_{loc}^2(\xi, \beta(\xi)) > M_{loc}^2(\xi, \beta_L)$. We predict nonequilibrium dynamics on the scale of nanoseconds (see Fig. 6), which should be measurable by ultrafast spectroscopy techniques [42]. Experimental setups are discussed in the next section.

C. Experimental consequences

Focusing on the constant temperature profile for now, we emphasize the system's translation symmetry. As mentioned before, the spin susceptibility $Q_T(k, \omega)$ at temperature T is given by the Fourier transformation of the Green's function $G_{\beta_0}(x, t)$ with $\beta_0 = 1/(k_B T)$ in Eq. (6). In Fig. 1, we show the regularized spin susceptibility at $T = 15$K as an example, and the related calculation is in Appendix B. The spin susceptibility has been measured already in neutron scattering experiments; see for instance [28]. From the spin susceptibility $Q_T(k, \omega)$, the Green's function can be obtained by the inverse Fourier transformation

$$G_{\beta_0}(x, t) = \int \frac{d\omega}{2\pi} \int \frac{dk}{2\pi} Q_T(k, \omega) e^{-i\omega t + ikx}, \qquad (14)$$

and therefore $G_{\beta_0}(0, 0) = \int d\omega \int dk \, Q_T(k, \omega)/(2\pi)^2$. According to Eq. (7), in the presence of translation symmetry, $G_{\beta_0}(0, 0) = g_0 + M_{loc}^2(\beta_0)$ holds for any specific position x
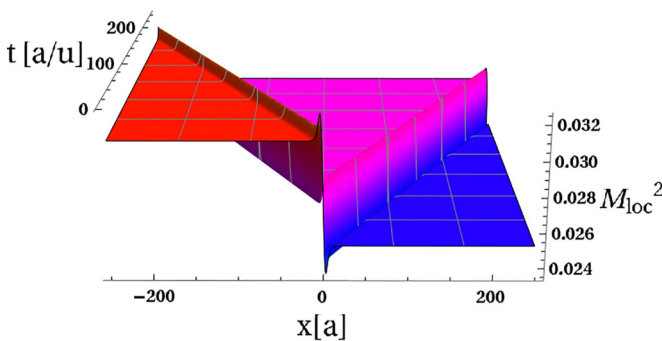

FIG. 6. $M_{loc}^2(\xi, \beta(\xi))$ from (13) is depicted for temperature profile $\beta_1(x)$ in CuPzN over a region $x \in [-\ell, \ell]$ with $\ell = 250a$ with $a = 6.7$ Å. The parameters are $T_L = 5$K (hot), $T_R = 4.5$K (cold), $\delta = 4a$. Time is measured in units $a/u \approx 0.5$ ps. The explicit form of the Schwarzian, (12), was employed.

and time t, and g_0 is a constant independent of temperature. The quantity $M_{loc}^2(\beta_0)$ carries the information of the central charges c and $\bar{\mathsf{c}}$ [see Eq. (8)], i.e., it corresponds to the conformal anomaly. Therefore, we have the following relation between the integrated spin susceptibility and the local magnetization, which in turn contains the central charge:

$$\int^\Lambda \frac{d\omega}{2\pi} \int \frac{dk}{2\pi} Q_T(k, \omega) = g_0 + M_{loc}^2 \qquad (15)$$

$$= g_0 + \frac{Ka^2}{3(u\hbar\beta_0)^2}(\mathsf{c} + \bar{\mathsf{c}}).$$

One observes that a natural way to obtain c from a spin system is to measure $Q_T(k, \omega)$ in neutron scattering experiments and integrate it in both momentum k and energy $\hbar\omega$. We introduced the upper limit Λ in the ω integration in Eq. (15) because spin susceptibility might include other contributions independent of the central charge, for instance high-energy modes.

We suggest two alternative ways of accessing the central charge in spin systems. For example, one can measure the local fluctuations $G_{\beta_0}(0, t)$ by NMR [43,44], AFM [45], or muon spin spectroscopy (μSR) [46] to obtain the *local dynamical structure factor* $\Gamma(\omega) = \int G_{\beta_0}(x, t; x, 0)e^{i\omega t} dt$. It is related to $Q_T(k, \omega)$ by a momentum integration $\Gamma(\omega) = \int dk \, Q_T(k, \omega)$. Taking NMR as an example, instead of taking the detailed information of $Q_T(k, \omega)$, the momentum-integrated quantity $\Gamma(\omega)$ is extracted from experiment: the so-called NMR relaxation rate $1/T_1$ is given by [47–50]

$$\frac{1}{T_1} = \frac{\gamma^2 A_H^2}{2} \int dk Q_T(k, \omega), \qquad (16)$$

with γ the nuclear gyromagnetic ratio, and A_H the hyperfine coupling constant.

Generally speaking, the function $\Gamma(\omega)$ extracted from the NMR relaxation rate $1/T_1$ depends on the nuclear Larmor frequency ω [51,52], which can be tuned by the magnetic field B through $\omega = \gamma B$, with $\gamma = qg/(2m)$, q is the nuclear charge, m is the nuclear mass, and g is the g-factor [53]. Therefore, if one varies the magnetic field from 0 to B_{max}, with $\omega_{max} = \gamma B_{max}$, one obtains the quantity

$$\int_0^{\omega_{max}} d\omega \, \Gamma(\omega). \qquad (17)$$

If the value of $\hbar\omega_{max}$ is several times that of $k_B T$, according to Appendix C, we can simply write

$$\int_0^{\omega_{max}} d\omega \, \Gamma(\omega) = \frac{Ka^2}{3u\hbar}(\mathsf{c} + \bar{\mathsf{c}})T^2 + \text{const}, \qquad (18)$$

in which the constant does not depend on temperature. The maximum frequency ω_{max} plays the role of the upper limit Λ of the integration in Eq. (15).

NMR explores the frequency region around $\omega = 0$ [49]. In order to reach the energy range up to $\hbar\omega_{max}$, we suggest to use electron paramagnetic resonance (EPR), which replaces the nuclear resonance with electron resonance. Due to the mass of the electron being approximately 2000 times smaller than that of the proton, the Larmor frequency is much higher in EPR that in NMR. Therefore, it may be useful to combine the information of $\Gamma(\omega)$ in the high frequency region from EPR

and the $\Gamma(\omega)$ data in the low frequency region from NMR. Then we can obtain the information of the central charge, according to Eq. (18).

Another way to detect the central charge is to measure the equal-time correlation by neutron diffraction, where one obtains the energy-integrated momentum dependent structure factor $\Sigma(k) = \int Q_T(k, \omega)d\omega$. Integrating k over the Brillouin zone $(-\pi/a, \pi/a)$,

$$\int_{-\pi/a}^{+\pi/a} dk\, \Sigma(k) = \frac{Ka^2}{3u\hbar}(\mathsf{c} + \bar{\mathsf{c}})T^2, \qquad (19)$$

produces the central charge. Furthermore, the information of $\Sigma(k)$ around $k = 0$, i.e., $\int Q_T(0, \omega)d\omega$, can be obtained by small-angle neutron scattering or by noise measurement. We elaborate briefly on the noise measurement. The average spin along the z axis is denoted by $\mathcal{S} = (\sum_i S_i^z/N)$ where i labels the site of the spin and N is the total number of the spins. The noise measures the correlation function $\langle \mathcal{S}(t)\mathcal{S}(0)\rangle$ between time t and 0 [54,55]. Noticing that

$$\frac{1}{N^2}\sum_{i,j}\langle S_i^z(t)S_j^z(0)\rangle = \frac{1}{L}\int dx G_{\beta_0}(x, t), \qquad (20)$$

one observes that the Fourier transformation of the correlation function $\langle \mathcal{S}(t)\mathcal{S}(0)\rangle$ measures $Q_T(0, \omega)$; see Appendix C for details.

Now we turn to nonuniform (but static) temperature profiles discussed in Sec. III B. Both ends of the spin chain are in contact with heat reservoirs of different temperatures, T_L and T_R. After a while, the system reaches a steady state, such that the temperature profile does not change significantly with time. At this time, which we call $t = 0$, a nontrivial temperature profile $T(x) = [k_B\beta(x)]^{-1}$ required for the discussion of Sec. III B arises. The variance of local magnetization M_{loc}^2 becomes (13). Furthermore, with $t = 0$ fixed, M_{loc}^2 is a function of the spatial coordinate and remains fixed (static) as long as the temperature profile is stable. M_{loc}^2 assumes the $t = 0$ form depicted in Fig. 6.

The case $t < 0$ represent the process in which the system approaches its stationary state. When the system reaches said stationary state, the physical observables do not change essentially with time, but they have spatial dependence. In order to detect the space dependent effects, one can perform the local measurement described above to obtain the local dynamical structure factor, which leads to Eq. (18) but the temperature T in the right-hand side will be replaced by the temperature profile in the final (steady) state $T(x)$. One can also measure the equal-time structure factor along the whole sample, e.g., by neutron diffraction, to obtain some similar result as in Eq. (19).

Next, we turn to the situation where the heaters are turned off. This corresponds to $t = 0$ in Fig. 6. For $t > 0$, the system starts to evolve into constant temperature state, visible in the pink region of Fig. 6. As time progresses this region spreads over the sample. This occurs within $\ell/u \sim$ nanoseconds where ℓ is the range of observation satisfying $\ell \gg \delta$. Experimentally this can be investigated via ultrafast laser spectroscopy [42] in the nanosecond spectrum range (see our predictions in Fig. 6) via a pump-and-probe approach. This is reflected in

optical properties such as reflectivity, absorption, or Raman scattering.

IV. CONCLUSIONS

In this paper, we have shown the presence of the conformal anomaly in finite temperature spin-spin correlators $G_\beta(\xi_1; \xi_2)$, concretely the normalized variance of local magnetization M_{loc}^2. This allows us to access the anomaly, more specifically the central charge, in a pure spin observable. We stress that our results are analytical even for strongly interacting 1D spin systems, and can be applied when the Luttinger paramaters K and u are known. Finally, we discussed experimental setups to probe the central charge and thus the conformal anomaly. For a constant temperature profile, $M_{\text{loc}}^2 \propto \mathsf{c}T^2$. The local magnetization can be measured in NMR, μSR, and neutron diffraction as long as the massless Luttinger liquid is a good description of the spin system. Moreover, we showed how the application of temperature gradients across the sample introduces space and time dependence in the local magnetization M_{loc}^2; see (13). In particular, the signal is enhanced in a small neighborhood of the temperature kink at $x = 0$. In spin chains with a steady but nonuniform temperature profile, one could measure a space-dependent local dynamical structure factor or could detect the magnetization dynamics in the ultrafast laser spectroscopy.

While we focused on spin-1/2 chains and ladders, it would be interesting to see if our results can be extended to spin systems of spin $s > 1/2$, which are associated with Wess-Zumino-Witten models [20]. Another interesting possibility is to extend our findings to higher order moments $\langle S^z(0)\partial_t S^z(\xi)\rangle$, which may be accessible experimentally. Another direction is to consider space-dependent magnetic fields by exploiting the fact that these translate into space-dependent chemical potentials.

APPENDIX A: THE CENTRAL CHARGE AND THE ENERGY-MOMENTUM TENSOR

In CFT, there is a special class of fields, called primary fields, labeled by left- and right-moving conformal weights $(h, \bar{h})$. These are the scaling fields of the CFT due to their characteristic transformation behavior under conformal

transformations $z \to g(z)$,

$$\chi_{h,\bar{h}}(g(z), \bar{g}(\bar{z})) = \left(\frac{\partial g}{\partial z}\right)^{-h} \left(\frac{\partial \bar{g}}{\partial \bar{z}}\right)^{-\bar{h}} \chi_{h,\bar{h}}(z, \bar{z}), \quad \text{(A1)}$$

where $g(z)$ is a holomorphic function of z. Primary fields organize the spectrum in that they are the ground states of so-called conformal towers, and the set of all conformal towers comprises the full Hilbert space of the CFT. In a free boson theory, such as the Luttinger liquid, one can easily write down two such fields. Starting from $\varphi(z, \bar{z}) = \phi(z) + \bar{\phi}(\bar{z})$, the derivatives $\partial \phi$ and $\bar{\partial} \bar{\phi}$ are primary with conformal weights $(h, \bar{h}) = (1, 0)$ and $(h, \bar{h}) = (0, 1)$, respectively. Together they provide $\partial_x \varphi$ in (2). But also the identity field **1** and the cosine term in (2) are primary fields. Hence in the next section we study the details of correlators of primaries. Before that, however, we take a closer look at the energy-momentum tensor.

The left-moving energy-momentum tensor $T(z)$ has dimensions $(h, \bar{h}) = (2, 0)$ while the right-moving component $\bar{T}(\bar{z})$ has dimensions $(h, \bar{h}) = (0, 2)$. Due to the conformal anomaly, both fail to transform according to (A1),

$$T(g(z)) = \left(\frac{\partial g}{\partial z}\right)^{-2} \left[T(z) - \frac{\mathsf{c}}{12}(Sg)(z)\right],$$

$$\bar{T}(\bar{g}(\bar{z})) = \left(\frac{\partial \bar{g}}{\partial \bar{z}}\right)^{-2} \left[\bar{T}(\bar{z}) - \frac{\bar{\mathsf{c}}}{12}(S\bar{g})(\bar{z})\right], \quad \text{(A2)}$$

with Schwarzian derivative

$$(Sg)(z) = \frac{g'''(z)}{g'(z)} - \frac{3}{2}\left(\frac{g''(z)}{g'(z)}\right)^2. \quad \text{(A3)}$$

A transformation from a zero-temperature system, coordinatized by z, to a thermal ensemble with temperature $1/\beta_0$, coordinatized by w, is

$$z = \exp\left(\frac{2\pi i w}{u\hbar\beta_0}\right), \quad w = \frac{u\hbar\beta_0}{2\pi i} \ln z, \quad \bar{z} = \exp\left(-\frac{2\pi i \bar{w}}{u\hbar\beta_0}\right), \quad \bar{w} = -\frac{u\hbar\beta_0}{2\pi i} \ln \bar{z}. \quad \text{(A4)}$$

It has Schwarzian derivative $(Sw)(z) = \frac{1}{2z^2}$, so that

$$T_{\beta_0}(w) = -\left(\frac{2\pi}{u\hbar\beta_0}\right)^2 \left[T_{\text{plane}}(z)z^2 - \frac{u\hbar\,\mathsf{c}}{24}\right],$$

$$\bar{T}_{\beta_0}(\bar{w}) = -\left(\frac{2\pi}{u\hbar\beta_0}\right)^2 \left[\bar{T}_{\text{plane}}(\bar{z})\bar{z}^2 - \frac{u\hbar\,\bar{\mathsf{c}}}{24}\right], \quad \text{(A5)}$$

where we indicate the geometry on which the T are defined by subscripts. Note that we reinstated $u\hbar$ as prefactors of c and $\bar{\mathsf{c}}$ for dimensional reasons. These expressions lead to a very simple evaluation of the expectation value of the energy-momentum tensor in a thermal ensemble. Indeed, fixing our reference energy such that $\langle T_{\text{plane}}(z)\rangle = 0$, one easily finds

$$\langle T(w)\rangle_{\beta_0} = \left(\frac{\pi}{\beta_0}\right)^2 \frac{\mathsf{c}}{6u\hbar}, \quad \langle \bar{T}(\bar{w})\rangle_{\beta_0} = \left(\frac{\pi}{\beta_0}\right)^2 \frac{\bar{\mathsf{c}}}{6u\hbar}, \quad \text{(A6)}$$

where we have moved the subscript on T_{β_0} to the expectation value in order to conform with the notation in the main text. Hence, the expectation value of the energy-momentum tensor is given entirely by the Schwarzian derivative term.

Since conformal transformations form a group, the Schwarzian derivative does as well, meaning that concatenations of Schwarzian derivatives are again described by a Schwarzian derivative. This is relevant in turning to the nonconstant temperature case described in Sec. III B. There, the geometry of nonconstant temperature $1/\beta(x)$ is first mapped into one with constant average temperature β_{av} and thereafter, similarly to just now, into a zero-temperature system.

Evaluating the Schwarzian derivative contribution in this scenario provides readily Eqs. (11) where the Schwarzian derivative (A3) evaluated on (10), adapted here to Euclidean

coordinates,

$$y = f(w) = \int_0^w \frac{\beta_{\text{av}}}{\beta(s)} ds, \quad \bar{y} = f(\bar{w}) = \int_0^{\bar{w}} \frac{\beta_{\text{av}}}{\beta(\bar{s})} d\bar{s}, \quad \text{(A7)}$$

yields

$$Sf(s) = \frac{1}{2}\left(\frac{\beta'(s)}{\beta(s)}\right)^2 - \frac{\beta''(s)}{\beta(s)}. \quad \text{(A8)}$$

as written in Sec. III B. The energy-momentum tensor is then

$$T_{\beta(w)}(w) = \left(\frac{\partial f(w)}{\partial w}\right)^2 T_{\beta_0}(f(w)) + \frac{\mathsf{c}}{12} Sf(w)$$

$$= -\left(\frac{2\pi}{\beta(w)u\hbar}\right)^2 T_{\text{plane}}(z)\, z^2$$

$$+ \left(\frac{\pi}{\beta(w)}\right)^2 \frac{\mathsf{c}}{6u\hbar} + \frac{u\hbar\,\mathsf{c}}{12} Sf(w) \quad \text{(A9)}$$

and similarly for $\bar{T}$. In going to the second line Eq. (A5) and $\frac{\partial f}{\partial w} = \frac{\beta_0}{\beta(w)}$ were employed. When taking the expectation value, $\langle T_{\text{plane}}(z)\rangle = 0$ almost results in (11) after $w \to w_-$ and $T \to T_-$. We note here without derivation that the Schwarzian $Sf(w)$ picks up an extra sign when Wick rotating, $Sf(w) \to -Sf(w_-)$ This game is repeated for $\bar{T} \to T_+$ with $\bar{w} \to w_+$, leading to (11) [40]. Our derivation here is the Euclidean time analog.

There is an important caveat when translating our Euclidean derivation to real time stemming from a subtlety in Wick rotating [40]: The expectation value of the energy-momentum tensor picks up an additional Schwarzian-like contribution stemming from the curvature of the deformed cylinder in Fig. 5 when switching between real and imaginary time. Working strictly in either real or imaginary time from the start, these contributions do not appear. Since we are

interested in settings in Minkowski spacetime, we worked with real time in Sec. III B. For proof of principle, here we stick with Euclidean time, to show that everything may be computed directly either in real or imaginary time.

APPENDIX B: CORRELATORS

Conformal symmetry constraints two-point functions at zero temperature to be

$$\langle \chi_{h_1,\bar{h}_1}(z_1,\bar{z}_1)\, \chi_{h_2,\bar{h}_2}(z_2,\bar{z}_2)\rangle = \mathcal{N}\frac{\delta_{h_1,h_2}}{(z_1-z_2)^{2h_1}}\frac{\delta_{\bar{h}_1,\bar{h}_2}}{(\bar{z}_1-\bar{z}_2)^{2\bar{h}_1}}. \tag{B1}$$

The constant $\mathcal{N}$ is a normalization for each operator and usually it is chosen to be 1. Here, it is left undetermined, so that the reader may adapt this to their favorite conventions.

For primaries, correlators at finite temperature can easily be obtained from (B1) by using the transformation (A1) together with the thermalizing conformal transformation (A4). This yields

$$\langle \chi_1(w_1,\bar{w}_1)\chi_2(w_2,\bar{w}_2)\rangle_{\beta_0}$$
$$= \mathcal{N}\left(\frac{\pi}{u\beta_0\hbar}\right)^{2(h_1+\bar{h}_1)}\sigma(w_1-w_2)^{-2h_1}\sigma(\bar{w}_1-\bar{w}_2)^{-2\bar{h}_1}\delta_{\bar{h}_1,\bar{h}_2}, \tag{B2}$$

where $\sigma(w)=\sin(\frac{\pi w}{u\beta_0\hbar})$. This opens the door to the computation of (5),

$$G_{\beta_0}(\xi_1,\xi_2) = \langle S^z(\xi_1)S^z(\xi_2)\rangle_{\beta_0} - \langle S^z(\xi_1)\rangle_{\beta_0}\langle S^z(\xi_2)\rangle_{\beta_0} \tag{B3}$$

$$= a^2\hbar^2\left\langle\frac{\partial_x\varphi(\xi_1)}{2\pi R}\frac{\partial_x\varphi(\xi_2)}{2\pi R}\right\rangle_{\beta_0} + a^2\hbar^2\left\langle\frac{1}{\pi}:\cos\left(\frac{\varphi(\xi_1)}{R}-2k_F(h)x_1\right): \frac{1}{\pi}:\cos\left(\frac{\varphi(\xi_2)}{R}-2k_F(h)x_2\right):\right\rangle_{\beta_0} \tag{B4}$$

$$= K\left(\frac{a}{2\beta_0 u}\right)^2[\sigma(w_1-w_2)^{-2}+\sigma(\bar{w}_1-\bar{w}_2)^{-2}] + \hbar^2\frac{\lambda a^2}{(2\pi)^2}\left(\frac{\pi}{\beta_0 u\hbar}\right)^{2K}$$
$$\times \sigma(w_1-w_2)^{-K}\sigma(\bar{w}_1-\bar{w}_2)^{-K}2\cos[k_F(h)(x_1-x_2)] \tag{B5}$$

with a model dependent constant λ accounting for the contributions of $\cos\phi$ operator in S^z. In going to the second line, (2) and $\langle S^z(w_2)\rangle_{\beta_0} = m$ were employed, together with the fact that none of the fields in S^z have the same conformal weights $(h,\bar{h})$. Therefore, there are no cross-correlators between fields; for instance $\langle\partial_x\varphi:\cos(\frac{\varphi(w_1)}{R}-2k_F(h)x_1):\rangle = 0$. Using

$$\frac{\partial_x\varphi(w)}{2\pi R}=\sqrt{K}[J(w)+\bar{J}(\bar{w})] \tag{B6}$$

and the fact that $J=\frac{i}{\sqrt{\pi}}\partial\varphi$ has $(h,\bar{h})=(1,0)$ and $\bar{J}=-\frac{i}{\sqrt{\pi}}\bar{\partial}\varphi$ has $(h,\bar{h})=(0,1)$ as well as $h=\bar{h}=K/2$ for the cosine operator, the result (B5) is straightforwardly derived through application of (B2). The correlator of the cosine operators is best handled by writing them in terms of exponentials and using the global $U(1)$ symmetry of the model which constrains correlators according to $\langle e^{i\alpha\varphi(z_1)}e^{i\beta\varphi(z_2)}\rangle \propto \delta_{\alpha+\beta,0}$.

Using expansions as in (4) on the full correlator (B5), it is possible to take the limit for the on-site variance (7),

$$M_{\text{loc}}^2(\xi,\beta_0) = \lim_{\xi'\to\xi}\frac{1}{S_{\max}^2}[\langle S^z(\xi)S^z(\xi')\rangle_{\beta_0} - \langle S^z(\xi)\rangle_{\beta_0}\langle S^z(\xi')\rangle_{\beta_0} - (\langle S^z(\xi)S^z(\xi')\rangle_\infty - \langle S^z(\xi)\rangle_\infty\langle S^z(\xi')\rangle_\infty)]$$

$$= \lim_{\xi'\to\xi}\frac{\hbar^2 a^2}{S_{\max}^2}\left[\frac{K}{(2\pi)^2}\frac{1}{(w-w')^2} + \frac{K}{(2\pi)^2}\frac{1}{(\bar{w}-\bar{w}')^2} + \frac{1}{(2\pi)^2}\frac{\lambda}{|w-w'|^{2K}} + \frac{K\mathsf{c}}{12(u\beta_0\hbar)^2} + \frac{K\bar{\mathsf{c}}}{12(u\beta_0\hbar)^2}\right.$$

$$\left. + \mathcal{O}(w-w') - \left(\frac{K}{(2\pi)^2}\frac{1}{(w-w')^2} + \frac{K}{(2\pi)^2}\frac{1}{(\bar{w}-\bar{w}')^2} + \frac{\lambda}{(2\pi)^2}\frac{1}{|w-w'|^{2K}}\right)\right]$$

$$= \frac{2Ka^2}{u\hbar\pi^2}[\langle T(w)\rangle_{\beta_0} + \langle\bar{T}(\bar{w})\rangle_{\beta_0}]. \tag{B7}$$

As mentioned above, the cosine term in (2) is not neglected on physical grounds but does in fact not contribute to M_{loc}^2 in the first place, as seen here by the cancellation of the terms proportional to λ. Moreover, the only contribution is due to the central charge, i.e., this result is entirely quantum in nature. This confirms that the construction of (7) is a very natural way of extracting the central charge in correlations, as all other data are projected out.

This calculation allows one to distinguish M_{loc}^2 clearly from existing quantities employing the correlator (5). For instance the susceptibility, as defined in [56], is given by

$$\overline{G}_{\beta_0} = \frac{\beta_0}{8\pi^2}\int_{-\infty}^{\infty}\left[\left(\frac{u\beta_0\hbar}{\pi}\sigma(w)\right)^{-2} + \left(\frac{u\beta_0\hbar}{\pi}\sigma(\bar{w})\right)^{-2}\right]dx, \tag{B8}$$

where we recall $w = u\tau - ix$ and $\bar{w} = u\tau + ix$. When $\tau \neq 0$ this expression can be evaluated yielding $\overline{G}_{\beta_0} = 1/(2\pi u)$. In order to see whether this expression secretly carries the central charge, it is necessary to recall that c can arise from $\sigma(w)^{-2}$ if $w \to 0$,

as seen from (7) and (8). By extension, (B8) needs to be evaluated at $\tau = 0$, in which case the anomaly contributes when the integration over x crosses $x = 0$. As it turns out, the integral over x does not converge in this limit. Therefore, this simple way of identifying the central charge c in $\overline{G}_{\beta_0}$ does not allow to extract a dependence on the central charge. It may nevertheless be that the anomaly sits in higher order terms of $\sigma(w)^{-2}$, but it is unclear how to extract such a dependence in $\overline{G}_{\beta_0}$. In contrast, the local magnetization M_{loc}^2 does contain the central charge c in a straightforward manner.

The analysis of (B7) can be repeated for the case of nonconstant temperature. First, a two point function is now found by the additional transformation (A7) relating constant and nonconstant temperature,

$$\langle \chi_1(w_1, \bar{w}_1)\chi_2(w_2, \bar{w}_2)\rangle_\beta = \prod_{i=1}^{2}\left(\frac{df}{dw}\right)^{h_i}\bigg|_{w=w_i}\left(\frac{df}{d\bar{w}}\right)^{\bar{h}_i}\bigg|_{\bar{w}=\bar{w}_i}\langle \chi_1(f(w_1), f(\bar{w}_1))\chi_2(f(w_2), f(\bar{w}_2))\rangle_{\beta_0}$$

$$= \mathcal{N}\left(\frac{\pi^2}{u^2\hbar^2\beta(w_1)\beta(w_2)}\right)^{h_1}\left(\frac{\pi^2}{u^2\hbar^2\beta(\bar{w}_1)\beta(\bar{w}_2)}\right)^{\bar{h}_1}\sin^{-2h_1}\left(\int_{w_2}^{w_1}\frac{\pi}{u\hbar\beta(s)}ds\right)$$

$$\times \sin^{-2\bar{h}_1}\left(\int_{\bar{w}_2}^{\bar{w}_1}\frac{\pi}{u\hbar\beta(\bar{s})}d\bar{s}\right)\delta_{h_1,h_2}\delta_{\bar{h}_1,\bar{h}_2}. \tag{B9}$$

This allows one to compute the analog of (4):

$$\langle \partial\varphi(w_1)\partial\varphi(w_2)\rangle_\beta = -\left(\frac{\sqrt{\pi}}{2u\hbar}\right)^2\frac{1}{\beta(w_1)\beta(w_2)}\sin^{-2}\left(\int_{w_2}^{w_1}\frac{\pi}{u\hbar\beta(s)}ds\right) \tag{B10a}$$

$$\overset{w_1\to w_2}{=} -\frac{1}{4\pi(w_1-w_2)^2} - \left[\frac{\pi}{12[u\hbar\beta(w_2)]^2} + \frac{1}{24\pi}\left\{\frac{1}{2}\left(\frac{\beta'(w_2)}{\beta(w_2)}\right) - \frac{\beta''(w_2)}{\beta(w_2)}\right\}\right] + \mathcal{O}((w_1-w_2)) \tag{B10b}$$

$$= -\frac{1}{4\pi(w_1-w_2)^2} - \left[\frac{\pi}{12[u\hbar\beta(w_2)]^2} + \frac{1}{24\pi}Sf(w_2)\right] + \mathcal{O}((w_1-w_2)). \tag{B10c}$$

Note again that, when Wick rotating, $Sf(w) \to -Sf(w_-)$. In contrast to the case of constant temperature, the Schwarzian derivative (A8) appears. The other difference is of course the replacement $\beta_0 \to \beta(w_2)$ in the first piece of the $\mathcal{O}((w_1 - w_2)^0)$ term. As before, by adjusting proportionality factors, the $\mathcal{O}((w_1 - w_2)^0)$ term is identified with $\langle T\rangle_\beta$, found in (11). Then, by the same logic that led up to (8) one can compute $M_{\text{loc}}^2(\xi, \beta(\xi))$. The analysis is identical, so one is free to simply plug (11) into (8), as mentioned in Sec. III B.

APPENDIX C: ABOUT THE UPPER BOUND OF THE ENERGY/MOMENTUM MEASUREMENT

In reality, measuring $Q_T(k, \omega)$ or $\Gamma(\omega)$ at $\omega = \infty$ is impractical. As in Eq. (18), one has to introduce a cutoff energy $\omega_{\max}$ as a truncation. How do we choose $\omega_{\max}$ to avoid huge errors when we try to measure the central charge? To answer this question, it is necessary to analyze the two-point Green's function

$$G_\beta(x, t) = \frac{Ka^2}{\pi}\frac{\text{Tr}(e^{-\beta H}\,\partial_x\phi(x, t)\,\partial_x\phi(0, 0))}{\text{Tr}(e^{-\beta H})}. \tag{C1}$$

With the help of mode expansion

$$\phi(x, t) = \int \frac{dp}{2\pi\sqrt{2\epsilon_p}}(a_p e^{-i\epsilon_p t + ipx} + a_p^\dagger e^{i\epsilon_p t - ipx}), \tag{C2}$$

we find that $G_\beta(x, t) = g(x, t) + \bar{G}_\beta(x, t)$, in which

$$g(x, t) = \frac{Ka^2}{\pi}\int \frac{dp}{4\pi\epsilon_p}p^2 e^{-i\epsilon_p t + ipx}, \tag{C3}$$

$$\bar{G}_\beta(x, t) = \frac{Ka^2}{\pi}\int \frac{dp}{2\pi\epsilon_p}p^2 n_B(\epsilon_p)\cos(\epsilon_p t - px). \tag{C4}$$

Only the latter function, $\bar{G}_\beta(x, t)$, carries the full temperature dependence. Comparing with Eqs. (7), (8), and (1), it becomes clear that $\bar{G}_\beta(x, t)$ contains the information of the central charge. One recognizes the Bosonic distribution function $n_B(\epsilon_p) = 1/(e^{\beta\epsilon_p} - 1)$, which decreases quickly as $\epsilon_p \gg k_B T$. After applying Fourier transformation to $\bar{G}_\beta(x, t)$, we obtained the spin susceptibility in momentum-energy coordinates,

$$\mathcal{G}_\beta(q, \omega) = \frac{Ka^2}{\pi}\frac{q^2}{2\epsilon_q}n_B(\epsilon_q)\delta(\omega - \epsilon_q), \tag{C5}$$

which is shown in Fig. 1.

[1] H. B. Nielsen and M. Ninomiya, The Adler-Bell-Jackiw anomaly and Weyl fermions in a crystal, Phys. Lett. B **130**, 389 (1983).

[2] D. Son and B. Spivak, Chiral anomaly and classical negative magnetoresistance of Weyl metals, Phys. Rev. B **88**, 104412 (2013).

[3] T. Dubček, C. J. Kennedy, L. Lu, W. Ketterle, M. Soljačić, and H. Buljan, Weyl points in three-dimensional optical lattices: Synthetic magnetic monopoles in momentum space, Phys. Rev. Lett. **114**, 225301 (2015).

[4] H.-Z. Lu and S.-Q. Shen, Weak antilocalization and localization in disordered and interacting Weyl semimetals, Phys. Rev. B **92**, 035203 (2015).

[5] C.-L. Zhang, S.-Y. Xu, I. Belopolski, Z. Yuan, Z. Lin, B. Tong, G. Bian, N. Alidoust, C.-C. Lee, S.-M. Huang *et al.*, Signatures of the Adler–Bell–Jackiw chiral anomaly in a Weyl fermion semimetal, Nat. Commun. **7**, 10735 (2016).

[6] C. Zhang, A. Narayan, S. Lu, J. Zhang, H. Zhang, Z. Ni, X. Yuan, Y. Liu, J.-H. Park, E. Zhang *et al.*, Evolution of Weyl orbit and quantum Hall effect in Dirac semimetal Cd_3As_2, Nat. Commun. **8**, 1272 (2017).

[7] J. Gooth, A. C. Niemann, T. Meng, A. G. Grushin, K. Landsteiner, B. Gotsmann, F. Menges, M. Schmidt, C. Shekhar, V. Süß *et al.*, Experimental signatures of the mixed axial–gravitational anomaly in the Weyl semimetal NbP, Nature (London) **547**, 324 (2017).

[8] R. Blumenhagen, D. Lüst, and S. Theisen, *Basic Concepts of String Theory*, Theoretical and Mathematical Physics (Springer, Heidelberg, 2013).

[9] P. Calabrese and J. Cardy, Entanglement entropy and conformal field theory, J. Phys. A **42**, 504005 (2009).

[10] G. Y. Cho, A. W. Ludwig, and S. Ryu, Universal entanglement spectra of gapped one-dimensional field theories, Phys. Rev. B **95**, 115122 (2017).

[11] S. Ryu and T. Takayanagi, Holographic derivation of entanglement entropy from the anti–de Sitter space/conformal field theory correspondence, Phys. Rev. Lett. **96**, 181602 (2006).

[12] G. Moore and N. Read, Nonabelions in the fractional quantum Hall effect, Nucl. Phys. B **360**, 362 (1991).

[13] D. Tong, Lectures on the quantum Hall effect, arXiv:1606.06687.

[14] G. Y. Cho, K. Shiozaki, S. Ryu, and A. W. Ludwig, Relationship between symmetry protected topological phases and boundary conformal field theories via the entanglement spectrum, J. Phys. A: Math. Theor. **50**, 304002 (2017).

[15] *Conformal Invariance and Applications to Statistical Mechanics*, edited by C. Itzykson, H. Saleur, and J. B. Zuber (World Scientific, Singapore, 1988).

[16] J. L. Cardy, Conformal invariance and statistical mechanics, in *Fields, Strings, Critical Phenomena, Proceedings of the Les Houches Summer School in Theoretical Physics, 1988* (North Holland, Amsterdam, 1989).

[17] P. Di Francesco, P. Mathieu, and D. Senechal, *Conformal Field Theory*, Graduate Texts in Contemporary Physics (Springer-Verlag, New York, 1997).

[18] D. Sénéchal, An introduction to bosonization, in *Theoretical Methods for Strongly Correlated Electrons* (Springer, Berlin, 2004), pp. 139–186.

[19] T. Giamarchi, *Quantum Physics in One Dimension*, International Series of Monographs on Physics Vol. 121 (Clarendon, Oxford, 2003).

[20] I. Affleck, Field theory methods and quantum critical phenomena, in *Cordes et Phénomènes Critiques (Fields, Strings and Critical phenomena)* (Elsevier, New York, 1989), pp. 564–640.

[21] J. C. Bonner and J. B. Parkinson, Quantum spin chains and the conformal anomaly, J. Appl. Phys. **63**, 3543 (1988).

[22] I. Affleck, Universal term in the free energy at a critical point and the conformal anomaly, in *Current Physics–Sources and Comments* (Elsevier, Amsterdam, 1988), Vol. 2, pp. 347–349.

[23] F. Heidrich-Meisner, A. Honecker, D. C. Cabra, and W. Brenig, Thermal conductivity of anisotropic and frustrated spin-1/2 chains, Phys. Rev. B **66**, 140406(R) (2002).

[24] E. Langmann, J. L. Lebowitz, V. Mastropietro, and P. Moosavi, Time evolution of the Luttinger model with nonuniform temperature profile, Phys. Rev. B **95**, 235142 (2017).

[25] M. Stone, Gravitational anomalies and thermal Hall effect in topological insulators, Phys. Rev. B **85**, 184503 (2012).

[26] B. Bermond, M. Chernodub, A. G. Grushin, and D. Carpentier, Anomalous Luttinger equivalence between temperature and curved spacetime: From black hole's atmosphere to thermal quenches, arXiv:2206.08784.

[27] P. Bouillot, C. Kollath, A. M. Läuchli, M. Zvonarev, B. Thielemann, C. Rüegg, E. Orignac, R. Citro, M. Klanjšek, C. Berthier *et al.*, Statics and dynamics of weakly coupled antiferromagnetic spin-1/2 ladders in a magnetic field, Phys. Rev. B **83**, 054407 (2011).

[28] D. Schmidiger, P. Bouillot, T. Guidi, R. Bewley, C. Kollath, T. Giamarchi, and A. Zheludev, Spectrum of a magnetized strong-leg quantum spin ladder, Phys. Rev. Lett. **111**, 107202 (2013).

[29] D. Blosser, V. K. Bhartiya, D. Voneshen, and A. Zheludev, $Z = 2$ quantum critical dynamics in a spin ladder, Phys. Rev. Lett. **121**, 247201 (2018).

[30] S. Galeski, K. Y. Povarov, D. Blosser, S. Gvasaliya, R. Wawrzynczak, J. Ollivier, J. Gooth, and A. Zheludev, *LT* scaling in depleted quantum spin ladders, Phys. Rev. Lett. **128**, 237201 (2022).

[31] L. Wu, S. Nikitin, Z. Wang, W. Zhu, C. D. Batista, A. Tsvelik, A. M. Samarakoon, D. A. Tennant, M. Brando, L. Vasylechko *et al.*, Tomonaga–Luttinger liquid behavior and spinon confinement in $YbAlO_3$, Nat. Commun. **10**, 698 (2019).

[32] S. E. Nikitin, S. Nishimoto, Y. Fan, J. Wu, L. Wu, A. Sukhanov, M. Brando, N. Pavlovskii, J. Xu, L. Vasylechko *et al.*, Multiple fermion scattering in the weakly coupled spin-chain compound $YbAlO_3$, Nat. Commun. **12**, 3599 (2021).

[33] O. Breunig, M. Garst, A. Klümper, J. Rohrkamp, M. M. Turnbull, and T. Lorenz, Quantum criticality in the spin-1/2 Heisenberg chain system copper pyrazine dinitrate, Sci. Adv. **3**, eaao3773 (2017).

[34] The same behavior is found when the CFT is given periodic boundary conditions with period L. In this case Eq. (1) carries over with $\beta_0 \to L$.

[35] D. C. Cabra and P. Pujol, Field-theoretical methods in quantum magnetism, in *Quantum Magnetism* (Springer, Berlin, 2008), pp. 253–305.

[36] A. Furusaki and S.-C. Zhang, Dynamical spin correlations in the Heisenberg ladder under a magnetic field and correlation functions in the $SO(5)$ ladder, Phys. Rev. B **60**, 1175 (1999).

[37] Readers might be worried about the appearance of the lattice constant a in this result, as it is a scale which is not taken into account in the CFT language. The lattice constant appears here due to the bosonization prescription (2). Basically, (2) remembers the lattice origin of the spin chain Hamiltonian, as it rightfully should, since this is the bridge between the lattice theory and the continuous low-energy effective QFT.

[38] M. Jeong, D. Schmidiger, H. Mayaffre, M. Klanjšek, C. Berthier, W. Knafo, G. Ballon, B. Vignolle, S. Krämer, A.

Zheludev *et al.*, Dichotomy between attractive and repulsive Tomonaga-Luttinger liquids in spin ladders, Phys. Rev. Lett. **117**, 106402 (2016).

[39] P. Hammar, M. Stone, D. H. Reich, C. Broholm, P. Gibson, M. Turnbull, C. Landee, and M. Oshikawa, Characterization of a quasi-one-dimensional spin-1/2 magnet which is gapless and paramagnetic for $g\mu_B H \lesssim J$ and $k_B T \ll J$, Phys. Rev. B **59**, 1008 (1999).

[40] K. Gawedzki, E. Langmann, and P. Moosavi, Finite-time universality in nonequilibrium CFT, J. Stat.. Phys. **172**, 353 (2018).

[41] D. Gutman, Y. Gefen, and A. Mirlin, Bosonization of one-dimensional fermions out of equilibrium, Phys. Rev. B **81**, 085436 (2010).

[42] T. Lee, F. Benesch, C. Reich, and C. G. Rose-Petruck, Ultrafast laser-pump X-ray probe measurements of solvated transition metal complexes, in *Femtochemistry VII* (Elsevier, Amsterdam, 2006), pp. 23–32.

[43] V. Herold, T. Kampf, and P. M. Jakob, Dynamic magnetic resonance scattering, Commun. Phys. **2**, 46 (2019).

[44] S. Capponi, M. Dupont, A. W. Sandvik, and P. Sengupta, NMR relaxation in the spin-1 Heisenberg chain, Phys. Rev. B **100**, 094411 (2019).

[45] A. Schwarz and R. Wiesendanger, Magnetic sensitive force microscopy, Nano Today **3**, 28 (2008).

[46] L. Nuccio, L. Schulz, and A. Drew, Muon spin spectroscopy: magnetism, soft matter and the bridge between the two, J. Phys. D: Appl. Phys. **47**, 473001 (2014).

[47] M. Randeria and A. A. Varlamov, Effect of superconducting fluctuations on spin susceptibility and NMR relaxation rate, Phys. Rev. B **50**, 10401(R) (1994).

[48] T. Suzuki and S. I. Suga, NMR relaxation of quantum spin chains in magnetic fields, Phys. Rev. B **74**, 172410 (2006).

[49] E. Coira, P. Barmettler, T. Giamarchi, and C. Kollath, Temperature dependence of the NMR spin-lattice relaxation rate for spin-1/2 chains, Phys. Rev. B **94**, 144408 (2016).

[50] M. Dupont, S. Capponi, and N. Laflorencie, Temperature dependence of the NMR relaxation rate $1/T_1$ for quantum spin chains, Phys. Rev. B **94**, 144409 (2016).

[51] M. Meyer, P. Maass, and A. Bunde, Spin-lattice relaxation: Non-Bloembergen-Purcell-Pound behavior by structural disorder and Coulomb interactions, Phys. Rev. Lett. **71**, 573 (1993).

[52] D. Kruk, R. Meier, and E. A. Rössler, Nuclear magnetic resonance relaxometry as a method of measuring translational diffusion coefficients in liquids, Phys. Rev. E **85**, 020201(R) (2012).

[53] E. A. Rainer Kimmich, Field-cycling NMR relaxometry, Prog. Nucl. Magn. Reson. Spectrosc. **44**, 257 (2004).

[54] A. Maeda, Noise study in condensed matter physics–towards extension to surrounding fields, J. Phys. Conf. Ser. **31**, 131 (2006).

[55] D. Roy, R. Singh, and R. Moessner, Probing many-body localization by spin noise spectroscopy, Phys. Rev. B **92**, 180205(R) (2015).

[56] S. Eggert, I. Affleck, and M. Takahashi, Susceptibility of the spin 1/2 Heisenberg antiferromagnetic chain, Phys. Rev. Lett. **73**, 332 (1994).